

Tunable electronic structures of germanane/antimonene van der Waals heterostructures using an external electric field and normal strain

Xing-Yi Tan(谭兴毅), Li-Li Liu(刘利利), Da-Hua Ren(任达华)

Citation: Chin. Phys. B . 2020, 29(7): 076102 . **doi:** 10.1088/1674-1056/ab8a39
Journal homepage: http://cpb.iphy.ac.cn; http://iopscience.iop.org/cpb

What follows is a list of articles you may be interested in

Theoretical study on order-disorder phase transition of $CH_3NH_3PbCl_3$

Jing Chang(常静), Zhen-Yi Jiang(姜振益), Qi Song(宋齐), Lei Chen(陈磊), Yan-Min Lin(林彦明), Bo Zhou(周波)
Chin. Phys. B . 2019, 28(11): 116105 . **doi:** 10.1088/1674-1056/ab478d

Isostructural phase transition-induced bulk modulus multiplication in dopant-stabilized ZrO_2 solid solution

Min Wang(王敏), Wen-Shu Shen(沈文舒), Xiao-Dong Li(李晓东), Yan-Chun Li(李延春), Guo-Zhao Zhang(张国召), Cai-Long Liu(刘才龙), Lin Zhao(赵琳), Shu-Peng Lv(吕舒鹏), Chun-Xiao Gao(高春晓), Yong-Hao Han(韩永昊)
Chin. Phys. B . 2019, 28(7): 076109 . **doi:** 10.1088/1674-1056/28/7/076109

Low temperature *Pmmm* and *C2/m* phases in $Sr_2CuO_{3+\delta}$ high temperature superconductor

Hai-Bo Wang(王海波), Zhen-Lin Luo(罗震林), Yuan-Jun Yang(杨远俊), Qing-Qing Liu(刘清青), Si-Xia Hu(胡思侠), Meng-Meng Yang(杨蒙蒙), Chang-Qing Jin(靳常青), Chen Gao(高琛)
Chin. Phys. B . 2019, 28(5): 056103 . **doi:** 10.1088/1674-1056/28/5/056103

High-pressure-induced phase transition in cinchomeronic acid polycrystalline form-I

Ting-Ting Yan(颜婷婷), Dong-Yang Xi(喜冬阳), Jun-Hai Wang(王俊海), Xu-Feng Fan(樊旭峰), Ye Wan(万晔), Li-Xiu Zhang(张丽秀), Kai Wang(王凯)
Chin. Phys. B . 2019, 28(1): 016104 . **doi:** 10.1088/1674-1056/28/1/016104

Compression behavior and phase transition of *β*-Si_3N_4 under high pressure

Hong-xia Gong(龚红霞), Zi-li Kou(寇自力), Cong Fan(樊聪), Hao Liang(梁浩), Qi-ming Wang(王齐明), Lei-lei Zhang(张雷雷), Fang Peng(彭放), Ming Yang(杨鸣), Xiao-lin Ni(倪小林), Jing Liu(刘景)
Chin. Phys. B . 2018, 27(5): 056101 . **doi:** 10.1088/1674-1056/27/5/056101

Tunable electronic structures of germanane/antimonene van der Waals heterostructures using an external electric field and normal strain*

Xing-Yi Tan(谭兴毅)[1,†], Li-Li Liu(刘利利)[1], and Da-Hua Ren(任达华)[2]

[1] *Department of Physics, Chongqing Three Gorges University, Wanzhou* 404100, *China*
[2] *School of Information Engineering, Hubei Minzu University, Enshi* 445000, *China*

(Received 3 March 2020; revised manuscript received 13 April 2020; accepted manuscript online 17 April 2020)

Van der Waals (vdW) heterostructures have attracted significant attention because of their widespread applications in nanoscale devices. In the present work, we investigate the electronic structures of germanane/antimonene vdW heterostructure in response to normal strain and an external electric field by using the first-principles calculations based on density functional theory (DFT). The results demonstrate that the germanane/antimonene vdW heterostructure behaves as a metal in a [−1, −0.6] V/Å range, while it is a direct semiconductor in a [−0.5, 0.2] V/Å range, and it is an indirect semiconductor in a [0.3, 1.0] V/Å range. Interestingly, the band alignment of germanane/antimonene vdW heterostructure appears as type-II feature both in a [−0.5, 0.1] range and in a [0.3, 1] V/Å range, while it shows the type-I character at 0.2 V/Å. In addition, we find that the germanane/antimonene vdW heterostructure is an indirect semiconductor both in an in-plane biaxial strain range of [−5%, −3%] and in an in-plane biaxial strain range of [3%, 5%], while it exhibits a direct semiconductor character in an in-plane biaxial strain range of [−2%, 2%]. Furthermore, the band alignment of the germanane/antimonene vdW heterostructure changes from type-II to type-I at an in-plane biaxial strain of −3%. The adjustable electronic structure of this germanane/antimonene vdW heterostructure will pave the way for developing the nanoscale devices.

Keywords: germanane/antimonene vdW heterostructure, electronic structures, external electric field, strain, first-principles calculations

PACS: 61.72.uj, 71.15.Mb, 74.78.Fk **DOI:** 10.1088/1674-1056/ab8a39

1. Introduction

In recent years, following the successful applications of graphene,[1] considerable efforts have been made to develop the two-dimensional (2D) materials, including antimonene,[2–5] germanane,[6–8] transition metal halides (TMHs),[9–11] transition metal chalcogenides (TMCs),[12,13] and transition metal dichalcogenides (TMDs),[14–16] because they have new physical mechanisms and promise to be used to design the next generation of nanoscale devices.[14,15] However, the 2D materials that have been realized experimentally cannot be used in all cases. For example, the zero-bandgap characteristics of graphene limit its applications in switching devices, in contrast, BN is a typical insulator with a very large band gap.[17–19] To solve this problem, in recent years, researchers have found that two different 2D materials can be stacked vertically to construct a van der Waals (vdW) heterostructure that not only retains the excellent characteristics of the original 2D materials but also may present more peculiar physical properties because of the coupling effect between the two layers.[20–23] This approach has opened up a new way of studying nanoelectronic and optoelectronic devices and thus becoming a research hotspot.

Antimonene, a novel group-V elemental monolayer, has been fabricated by several experimental methods, including plasma-assisted process,[24] van der Waals epitaxy growth,[3] mechanical exfoliation,[24] and molecular beam epitaxy.[5,25–27] Antimonene offers excellent physical properties, such as high stability,[5] high thermal conductivity,[28] high carrier mobility,[5] and a suitably wide band gap[5,29] and thus having received a great deal of attention.[28,30,31] Wang *et al.*[28] found that antimonene with a buckled hexagonal phase is more stable, and that it has an indirect bandgap that is sensitive to strain. A few researches on antimonene-based vdW heterostructures have also been carried out. For example, Zhang *et al.*[32] found that the Sb/InSe vdW heterostructure has a robust type-II staggered-gap band alignment; the band gap can be tuned by using an external electric field and it is thus a potential candidate material for nanoelectronics. Wang *et al.*[33] found that the Sb/GaAs heterostructures have a type-II band alignment and small band gaps in a range of 0.71 eV–1.39 eV, which makes them potential candidate materials for being used in optoelectronic devices. Wang *et al.*[34] found that the C_2N/β-Sb vdW heterostructure also has a type-II band alignment and thus has great potential applications in designing the next generation of high-performance optoelectronic devices. These findings suggest that antimonene-based vdW heterostructures are strong potential candidate materials for optoelectronic de-

*Project supported by the National Natural Science Foundation of China (Grant No. 11864011).
†Corresponding author. E-mail: tanxy@sanxiau.edu.cn
© 2020 Chinese Physical Society and IOP Publishing Ltd

vices.

Germanane, *i.e.*, a monolayer of hydrogenated puckered germanium atoms, has recently been chemically synthesized[6] and has been widely investigated because of its direct band gap and high electron mobility.[35] Ghosh *et al.*[36] demonstrated that germanane gives a better performance in switching device applications than other 2D materials because it has a very low effective mass. Li and Chen[37] found that the band gap of the germanane is rather robust under the action of an external electronic field, but it is sensitive to biaxial tensile strain. Zhang *et al.*[38] reported that the band gap of a germanene/germanane heterostructure can be opened up under the action of an external electric field and strain. Nevertheless, a theoretical study for electronic structures of germanane/antimonene vdW heterostructures and applications in optoelectronic devices is sorely lacking. Here in this work, we investigate the electronic structures of germanane/antimonene vdW heterostructures in response to normal strain and an external electric field by using the first-principles calculations and found that a normal strain and an external electric field can tune the electronic structure of the germanane/antimonene vdW heterostructure.

2. Computational methods

All the research on germanane/antimonene vdW heterostructures was performed by using the first-principles calculations based on density functional theory (DFT). The generalized gradient approximation (GGA)[39,40] of the Perdew–Burke–Ernzerhof (PBE) functional was used for the crystal structure relaxation, which was implemented in the ATK simulation package.[41,42] The PseudoDojo method was used to solve the Kohn–Sham equations. The energy cutoff of 120 hartree (1 hartree = 4.3597×10^{-18} J) and the Brillouin zone sampling of the K-mesh of $7\times7\times1$ were adopted. For accuracy, a K-mesh of $9\times9\times1$ was used to perform the energy band structure calculations. In the relaxation, the energy criterion was 10^{-4} eV and the residual force was lower than -0.05 eV/Å. The vacuum layer thickness was more than 20 Å to prevent spurious interactions from occurring in the neighboring images. Significantly, the long-range vdW interaction was important in terms of holding the 2D vdW heterostructure together. Here, the vdW-DF2 functional was chosen to describe long-range electron correlation effects.[43]

3. Results and discussion

First, we optimize the crystal structures of the pristine germanane and antimonene monolayers. After relaxation, the lattice constant of the pristine germanane monolayer is 4.076 Å, which is consistent with the previous theoretical values of 4.06 Å and 4.09 Å reported by Zhang[38] and Garcia *et al.*,[44] respectively. The lattice constant of a pristine antimonene monolayer is 4.074 Å, which is consistent with the theoretical values of 4.12 Å and 4.08 Å previously reported by Lu[45] and Chen *et al.*,[46] respectively. Therefore, we construct the germanane/antimonene vdW heterostructures by using single unit cells of germanane and antimonene. The calculated lattice mismatch is 0.05%, which implies that the lattices match very well. To obtain the ground state, six stacking conformations are taken into account in this work, named model I, model II, ..., and model VI as shown in Fig. 1. The interface distance between two layers is defined as Δ, and the calculated values are listed in Table 1. It is obvious that model II has the shortest distance.

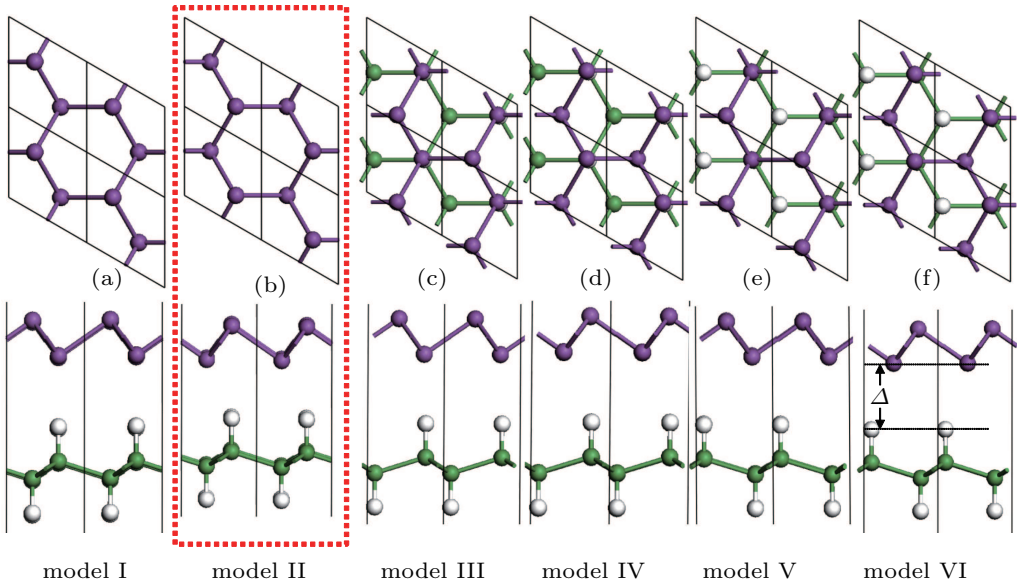


Fig. 1. Top and side views of the atomic model of germanane/antimonene vdW heterostructure ($2\times2\times1$ supercells) for (a) model I, (b) model II, (c) model III, (d) model IV, (e) model V, and (f) model VI, with Δ showing in model VI denoting interlayer distance, and Sb atoms of the antimonene and Ge and H atoms being represented by purple, green, and white balls, respectively. Also $2\times2\times1$ supercells are shown there.

Next, we calculate the binding energy (E_b) of the germanane/antimonene vdW heterostructure, which is defined as[32]

$$E_b = E_{total} - E_{ge} - E_{sb}, \quad (1)$$

where E_b represents the binding energy of the germanane/antimonene vdW heterostructure, and E_{total}, E_{ge}, and E_{sb} denote the total energy of the germanane/antimonene vdW heterostructure, the germanane monolayer, and the antimonene monolayer, respectively. The calculated E_b values are listed in Table 1. Apparently, model II has the lowest E_b, which means that model II is of the ground state. Therefore, all the research on germanane/antimonene van der Waals heterostructures in the following is only performed based on model II.

Table 1. Values of binding energy (E_b) and interface distance between two layers (Δ) for six stacking conformations.

Model	I	II	III	IV	V	VI
E_b/eV	−0.528	−0.561	−0.529	−0.540	−0.541	−0.538
Δ/Å	3.223	2.744	3.215	3.143	3.123	3.143

To understand the electronic structures of the germanane/antimonene vdW heterostructure, we calculate the electronic structures of pristine germanane, pristine antimonene and the germanane/antimonene vdW heterostructure as shown in Figs. 2(a)–2(c). For the pristine germanane, from Fig. 2(a), we find that both the conduction band minimum (CBM) and the valence band maximum (VBM) are located at the Γ point of the high symmetry point in the Brillouin zone (BZ); this indicates that the germanane monolayer shows direct semiconductor characteristics with a bandgap of 1.164 eV. This calculated result is similar to the theoretical values of 1.05 eV and 0.95 eV, obtained by Zhang *et al.*[38] and of Garcia *et al.*[44] through using the PBE functional, respectively. We observe that this value is smaller than the value of 1.56 eV[6] obtained by using the HSE06 method because the PBE method underestimates the band gap. For pristine antimonene, from Fig. 2(b) we find that the VBM is located at the Γ point, while the CBM lies on the line from Γ to M and is located close to the M point; this means that the antimonene presents indirect semiconductor characteristics with a gap value of 1.231 eV. This calculated result is approximately equal to the theoretical values of 1.227 eV and 1.245 eV reported by Zhang *et al.*[32] and Chen *et al.*[46] through using the PBE functional, respectively. Their small errors are due to the software package we used to perform the calculations. In the meantime, we also find that our value is smaller than the value (2.28 eV)[5] obtained by using the HSE06 method. In fact, the standard PBE functional enables the predicting of the correct tendencies of the band structures, thus appropriately demonstrating the physical mechanisms. To reduce the computational cost, we use the PBE method to calculate the electronic structures of the germanane/antimonene vdW heterostructures under theaction of electric field and strain. For the germanane/antimonene vdW heterostructure, from Fig. 2(c), the CBM mainly originates from the germanane monolayer, while the VBM mainly sources from the antimonene monolayer, and both are located at the Γ point; this indicates that the germanane/antimonene vdW heterostructure shows a unique type-II band alignment and that it is a direct band gap semiconductor with a band gap value of 0.769 eV.

To faciliate understanding the electronic structures of the germanane/antimonene vdW heterostructure, we depict the band alignment of the germanane/antimonene vdW heterostructure as shown in Fig. 2(d). This figure shows that the band edges of germanane and antimonene are (0.352, −0.792) eV and (0.839, −0.417) eV, respectively. The CBM and the VBM of the germanane monolayer are lower than those of the antimonene monolayer, which provides further the evidence of the type-II band alignment of the germanane/antimonene vdW heterostructure. The heterostructure can enable the electrons and holes to be separated from each other in real space and can thus be used to design the optoelectronic devices that inhibit carrier recombination.

Previous theoretical and experimental results have shown that the applied electric field can effectively regulate the electronic structures of the vdW heterostructure.[47–49] The electric field direction lies in the direction perpendicular to the germanane/antimonene vdW heterostructure, and the positive direction of the electric field points from germanane toward antimonene. The electric field is applied over the range from −1.0 V/Å to 1 V/Å in steps of 0.1 V/Å. The band gap, the energy band edges and the electronic structures of the germanane/antimonene vdW heterostructure *versus* applied electric field are shown in Fig. 3 and Fig. A1 in Appendix A, respectively. The germanane/antimonene vdW heterostructure is found to undergo a metal–semiconductor phase transition at −0.6 V/Å. The bandgap value increases linearly with electric field increasing in a [−0.5, 0.2] V/Å range, and decreases linearly with electric field increasing in a [0.2, 1.0] V/Å range. Additionally, the germanane/antimonene vdW heterostructure has direct semiconductor characteristics over the [−0.5, 0.2] V/Å range, and indirect semiconductor characteristics over the [0.3, 1.0] V/Å range. In addition, in a range of [−0.5, 0.1] V/Å, the CBM mainly comes from monolayer germanane, while VBM principally derives from monolayer antimonene, indicating a type-II band alignment. In a range of [0.3, 1.0] V/Å, the CBM primarily originates from monolayer antimonene, while the VBM mainly derived from monolayer germanane, indicating a type-II band alignment, too. Interestingly, when the electric field intensity is equal to 0.2 V/Å, both the conduction band and the valence band near Fermi level mainly come from monolayer germanane, manifesting a type-I band alignment. These findings indicate that the electronic structures of the germanane/antimonene vdW heterostructure can be tuned by applying an electric field.

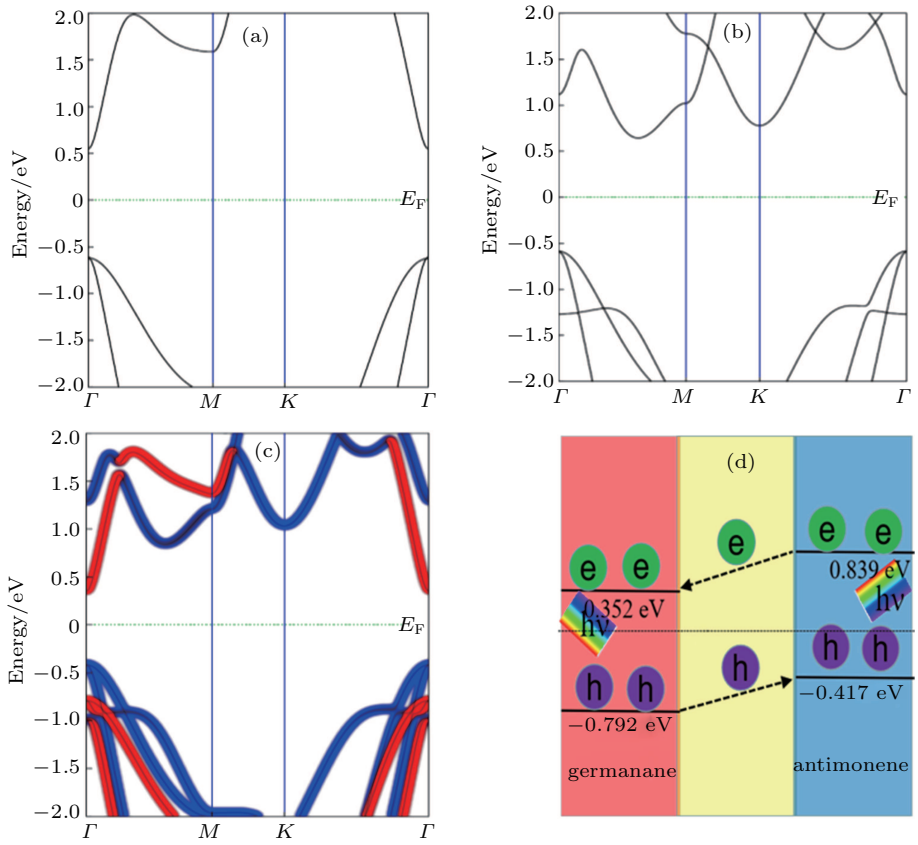


Fig. 2. Band structure of (a) pristine germanane, (b) pristine antimonene, and (c) model II of germanane/antimonene vdW heterostructure. (d) Band alignment of germanane/antimonene vdW heterostructure at PBE level. The Fermi level is set at 0 eV and is represented by black dashed line.

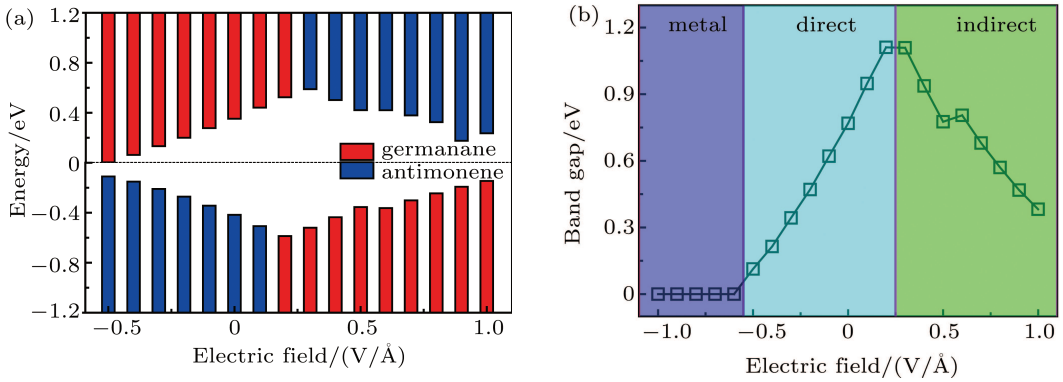


Fig. 3. (a) Band alignment and (b) band gap of the germanane/antimonene vdW heterostructure under action of applied electric field.

It has been demonstrated both experimentally and theoretically that strain can also be used to regulate the electronic structure of the vdW heterostructure.[49–52] Next, we study the electronic structure of the germanane/antimonene vdW heterostructure under the applied external strain. The in-plane biaxial strain on the germanane/antimonene vdW heterostructure is calculated by changing the crystal lattice constants and is defined by the following physical formula: $\Theta = [(a - a_0)/a_0] \times 100\%$, where a_0 and a represent the lattice constants in unstrained and under strained conditions, respectively. The external strain is applied over the range from -5% to 5% in steps of 1%. The strain effects on the band edges, the bandgap and the electronic structure of the germanane/antimonene vdW heterostructure are depicted in Figs. 4 and A2. From Fig. A2, we find that the VBM is located at the Γ point, while the CBM lies on the K point over the range of $[-5\%, -3\%]$; both the VBM and the CBM are located at the Γ point over the range of $[-2\%, 2\%]$; and the CBM is located at the Γ point, while the VBM lies on the line from Γ to M and is located close to the Γ point over the range of $[3\%, 5\%]$. These results mean that the germanane/antimonene vdW heterostructure is an indirect semiconductor over the ranges of $[-5\%, -3\%]$ and $[3\%, 5\%]$, while it is a direct semiconductor over the $[-2\%, 2\%]$ range.

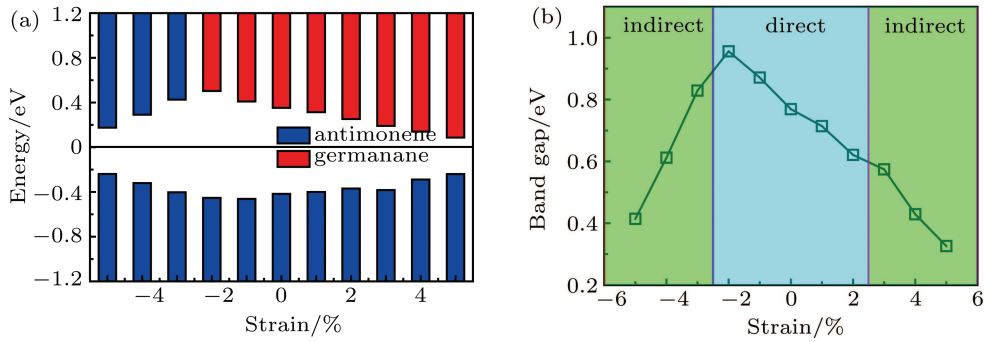


Fig. 4. (a) Band alignment and (b) band gap of germanane/antimonene vdW heterostructure under in-plane biaxial strain in steps of 1%.

In addition, the germanane/antimonene vdW heterostructure has a type-I band alignment over the [−5%, −3%] range, for both the CBM and the VBM are contributed by the antimonene monolayer, and it has a type-II band alignment over the [−3%, 5%] range, for the CBM is contributed by the germanane monolayer and the VBM is contributed by the antimonene monolayer. These findings indicate that the electronic structures of the germanane/antimonene vdW heterostructure can be tuned by strain.

4. Conclusions

In this work, we determine the electronic structures of the germanane/antimonene vdW heterostructure under an applied electric field and applied strain using first-principles calculations. It is demonstrated that the germanane/antimonene vdW heterostructure is a metal over the range from [−1, −0.6] V/Å, while it is a semiconductor over the range from [−0.5, 1.0] V/Å. Interestingly, the germanane/antimonene vdW heterostructure band alignment presents type-II feature in the ranges of $[-0.5, 0.1]$ V/Å and $[0.3, 1.0]$ V/Å, and type-I characteristic at 0.2 V/Å. In addition, the germanane/antimonene vdW heterostructure is an indirect semiconductor over the ranges of [−5%, −3%] and [3%, 5%], while it is a direct semiconductor over the [−3%, 3%] range. Furthermore, the germanane/antimonene vdW heterostructure band alignment changes from type-II to type-I at −3%. The tunable band gap of the germanane/antimonene vdW heterostructure is thus suitable for applications in band engineering and electronic device design.

Appendix A: Supplemental materials

The bad gap, the energy band edges, and the electronic structures of the germanane/antimonene vdW heterostructure are shown in Figs. A1 and A2.

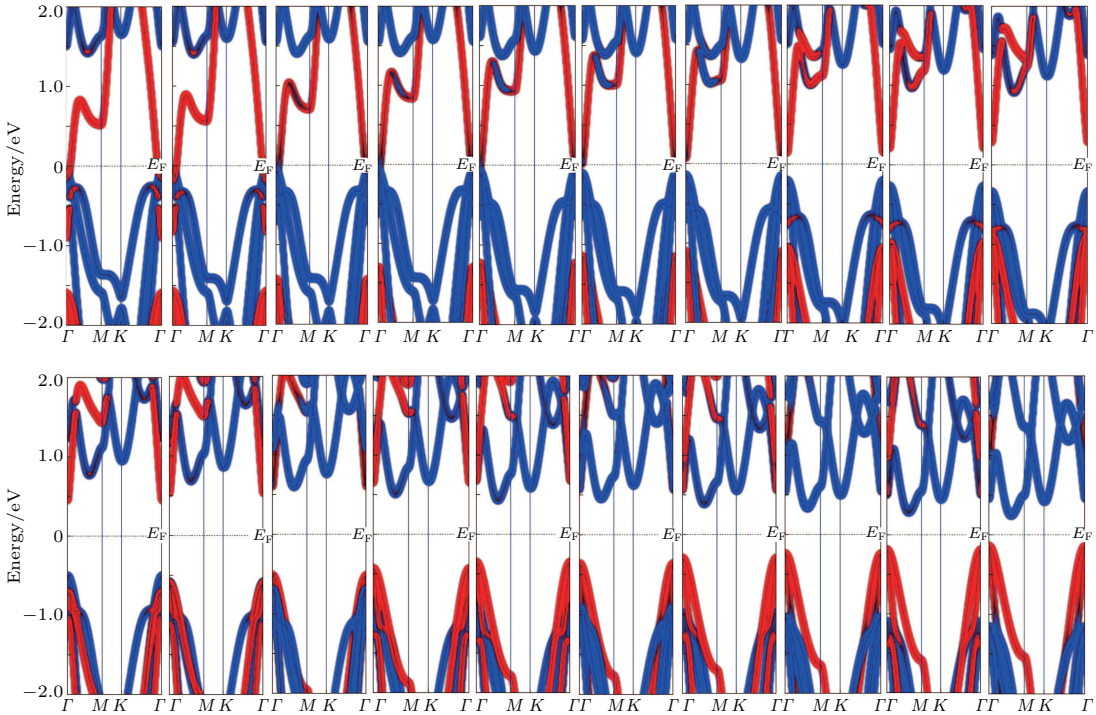


Fig. A1. Band structures of germanane/antimonene vdW heterostructure under applied electric fields in steps of 0.1 V/Å. The top half of the diagram represent −1 V/Å to −0.1 V/Å from left to right, and the bottom half of the diagram represent 0.1 V/Å to 1 V/Å from left to right. Red lines represent germanane, while blue lines denote antimonene.

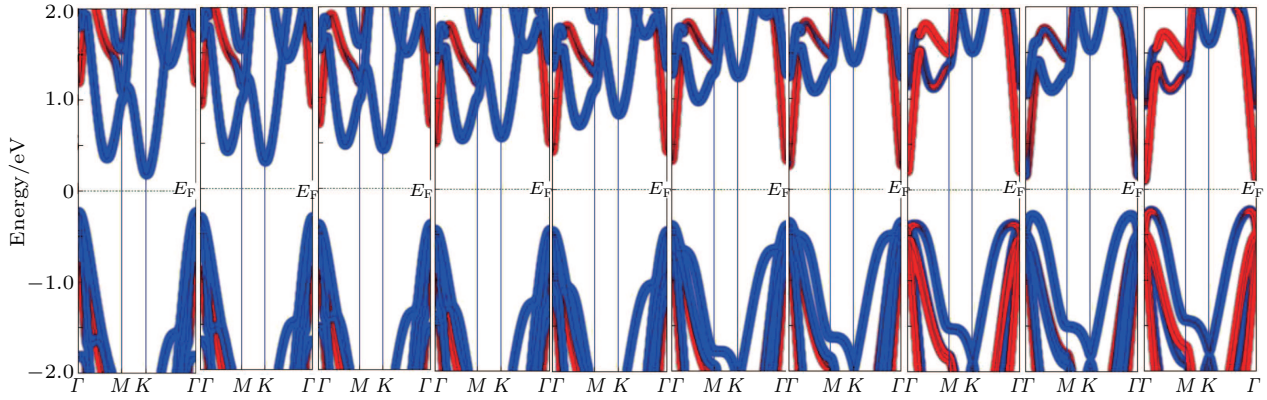


Fig. A2. Band structures of germanane/antimonene vdW heterostructure under in-plane biaxial strains in steps of 1%; from left to right, strains range from −5% to 5%. Red lines represent germanane, and blue lines denote antimonene.

References

[1] Novoselov K S, Geim A K, Morozov S V, Jiang D, Zhang Y, Dubonos S V, Grigorieva I V and Firsov A A 2004 *Science* **306** 666

[2] Gibaja C, Rodriguez-San-Miguel D, Ares P, Gómez-Herrero J, Varela M, Gillen R, Maultzsch J, Hauke F, Hirsch A and Abellán G 2016 *Angew. Chem. Int. Edit.* **55** 14345

[3] Ji J, Song X, Liu J, Yan Z, Huo C, Zhang S, Su M, Liao L, Wang W and Ni Z 2016 *Nat. Commun.* **7** 13352

[4] Singh D, Gupta S K, Sonvane Y and Lukačević I 2016 *J. Mater. Chem. C* **4** 6386

[5] Zhang S, Yan Z, Li Y, Chen Z and Zeng H 2015 *Angew. Chem. Int. Edit.* **54** 3112

[6] Bianco E, Butler S, Jiang S, Restrepo O D, Windl W and Goldberger J E 2013 *ACS Nano* **7** 4414

[7] Wei W, Dai Y, Huang B and Jacob T 2013 *Phys. Chem. Chem. Phys.* **15** 8789

[8] Madhushankar B, Kaverzin A, Giousis T, Potsi G, Gournis D, Rudolf P, Blake G, Van Der Wal C and Van Wees B 2017 *2D Mater.* **4** 021009

[9] Zhou L, Kou L, Sun Y, Felser C, Hu F, Shan G, Smith S C, Yan B and Frauenheim T 2015 *Nano Lett.* **15** 7867

[10] Huang C, Du Y, Wu H, Xiang H, Deng K and Kan E 2018 *Phys. Rev. Lett.* **120** 147601

[11] Huang C, Zhou J, Wu H, Deng K, Jena P and Kan E 2017 *Phys. Rev. B* **95** 045113

[12] Guo Y, Dai J, Zhao J, Wu C, Li D, Zhang L, Ning W, Tian M, Zeng X C and Xie Y 2014 *Phys. Rev. Lett.* **113** 157202

[13] Li S L, Tsukagoshi K, Orgiu E and Samorì P 2016 *Chem. Soc. Rev.* **45** 118

[14] Wang Q H, Kalantar-Zadeh K, Kis A, Coleman J N and Strano M S 2012 *Nat. Nanotechnol.* **7** 699

[15] Jariwala D, Sangwan V K, Lauhon L J, Marks T J and Hersam M C 2014 *ACS Nano* **8** 1102

[16] Qian X, Liu J, Fu L and Li J 2014 *Science* **346** 1344

[17] Liu L, Feng Y and Shen Z 2003 *Phys. Rev. B* **68** 104102

[18] Preobrajenski A, Nesterov M, Ng M L, Vinogradov A and Mårtensson N 2007 *Chem. Phys. Lett.* **446** 119

[19] Schedin F, Geim A K, Morozov S V, Hill E, Blake P, Katsnelson M and Novoselov K S 2007 *Nat. Mater.* **6** 652

[20] Geim A K and Grigorieva I V 2013 *Nature* **499** 419

[21] Novoselov K, Mishchenko A, Carvalho A and Neto A C 2016 *Science* **353** aac9439

[22] Liu Y, Weiss N O, Duan X, Cheng H C, Huang Y and Duan X 2016 *Nat. Rev. Mater.* **1** 16042

[23] Jariwala D, Marks T J and Hersam M C 2017 *Nat. Mater.* **16** 170

[24] Ares P, Aguilar-Galindo F, Rodríguez-San-Miguel D, Aldave D A, Díaz-Tendero S, Alcamí M, Martín F, Gómez-Herrero J and Zamora F 2016 *Adv. Mater.* **28** 6332

[25] Lei T, Liu C, Zhao J L, Li J M, Li Y P, Wang J O, Wu R, Qian H J, Wang H Q and Ibrahim K 2016 *J. Appl. Phys.* **119** 015302

[26] Fortin-Deschênes M, Waller O, Mentes T, Locatelli A, Mukherjee S, Genuzio F, Levesque P, Hébert A, Martel R and Moutanabbir O 2017 *Nano Lett.* **17** 4970

[27] Wu X, Shao Y, Liu H, Feng Z, Wang Y L, Sun J T, Liu C, Wang J O, Liu Z L and Zhu S Y 2017 *Adv. Mater.* **29** 1605407

[28] Wang G, Pandey R and Karna S P 2015 *ACS Appl. Mater. Inte.* **7** 11490

[29] Zhao M, Zhang X and Li L 2015 *Sci. Rep.* **5** 16108

[30] Ares P, Aguilar-Galindo F, Rodríguez-San-Miguel D, Aldave D A, Díaz-Tendero S, Alcamí M, Martín F, Gómez-Herrero J and Zamora F 2016 *Adv. Mater.* **28** 6515

[31] Pizzi G, Gibertini M, Dib E, Marzari N, Iannaccone G and Fiori G 2016 *Nat. Commun.* **7** 12585

[32] Zhang Z, Zhang Y, Xie Z, Wei X, Guo T, Fan J, Ni L, Tian Y, Liu J and Duan L 2019 *Phys. Chem. Chem. Phys.* **21** 5627

[33] Wang N, Cao D, Wang J, Liang P, Chen X and Shu H 2017 *J. Mater. Chem. C* **5** 9687

[34] Wang X, Quhe R, Cui W, Zhi Y, Huang Y, An Y, Dai X, Tang Y, Chen W and Wu Z 2018 *Carbon* **129** 738

[35] Li L, Lu S Z, Pan J, Qin Z, Wang Y Q, Wang Y, Cao G Y, Du S and Gao H J 2014 *Adv. Mater.* **26** 4820

[36] Ghosh R K, Brahma M and Mahapatra S 2014 *IEEE T. Electron. Dev.* **61** 2309

[37] Li Y and Chen Z 2014 *J. Phys. Chem. C* **118** 1148

[38] Zhang R W, Zhang C W, Ji W X, Li F, Ren M J, Li P, Yuan M and Wang P J 2015 *Phys. Chem. Chem. Phys.* **17** 12194

[39] Perdew J P, Burke K and Ernzerhof M 1996 *Phys. Rev. Lett.* **77** 3865

[40] Perdew J P and Wang Y 1992 *Phys. Rev. B* **45** 13244

[41] Brandbyge M, Mozos J L, Ordejón P, Taylor J and Stokbro K 2002 *Phys. Rev. B* **65** 165401

[42] ToolKit A 2014 S http://www.quantumwise.com

[43] Lee K, Murray E D, Kong L, Lundqvist B I and Langreth D C 2010 *Phys. Rev. B* **82** 081101

[44] Garcia J C, De Lima D B, Assali L V and Justo J F 2011 *J. Phys. Chem. C* **115** 13242

[45] Lu H, Gao J, Hu Z and Shao X 2016 *RSC Adv.* **6** 102724

[46] Chen X, Yang Q, Meng R, Jiang J, Liang Q, Tan C and Sun X 2016 *J. Mater. Chem. C* **4** 5434

[47] Wang S and Yu J 2018 *Thin Solid Films* **654** 107

[48] Wang S and Yu J 2018 *Appl. Phys. A* **124** 487

[49] Guo X, Li D and Xi L 2018 *Chin. Phys. B* **27** 097506

[50] Zhang P, Wang J and Duan X M 2016 *Chin. Phys. B* **25** 037302

[51] Wang S K and Jun W 2015 *Chin. Phys. B* **24** 037202

[52] Zhang L, He D W and He J Q 2019 *Chin. Phys. B* **28** 087201